Pergamon

Acta mater. Vol. 47, No. 1, pp. 67–76, 1999

Printed in Great Britain
PII: S1359-6454(98)00345-0
1359-6454/99 $19.00 + 0.00

SPLIT SINGULARITIES: STRESS FIELD NEAR THE EDGE OF A SILICON DIE ON A POLYMER SUBSTRATE

X. H. LIU[1], Z. SUO[1]† and Q. MA[2]

[1]Department of Mechanical and Aerospace Engineering, and Princeton Materials Institute, Princeton University, Princeton, NJ 08544, U.S.A. and [2]Components Research, Intel Corporation, Santa Clara, CA 95052, U.S.A.

(Received 5 August 1998; accepted 24 September 1998)

Abstract—In current design the circuitry is extended very close to the edges of a silicon die to maximize useful surface area. When the die is bonded to a polymer substrate, with the circuitry facing the polymer, thermal misfit stress concentrates at the die edges and may damage the circuitry. The stress distribution near a die edge is quantified using a combination of asymptotic analysis and finite element calculation. The asymptotic field consists of two modes of singular stresses, scaling with the distance from the edge r as, respectively, $r^{-\lambda_1}$ and $r^{-\lambda_2}$, where $\lambda_1 > \lambda_2$. It is shown that the more singular field (i.e. the λ_1-singularity) prevails in an exceedingly small zone, smaller than 10^{-6} times the die thickness. Once both modes are included, however, the asymptotic field matches the full field in a zone about 10^{-1} times the die thickness. This finding resolves several controversies in the literature on electronic packaging. The near-edge stress distribution is presented for various substrate thicknesses, elastic moduli and thermal expansion coefficients. The results can be used to explore design options. © *1998 Acta Metallurgica Inc. Published by Elsevier Science Ltd. All rights reserved.*

1. INTRODUCTION

As the semiconductor industry moved from ceramic to plastic packaging materials, new reliability problems developed. A host of failures resulted from the large thermal expansion mismatch between silicon dies and plastic substrates. Particularly severe is die–package debonding close to die edges, where thermal stresses concentrate. For traditional packaging configurations, the back of a die is bonded to a plastic substrate, so that debonding limited to the die edges is tolerable. However, for the flip-chip attachment (Fig. 1), the circuitry is on the interface, so that any debonding threatens electric signals. Furthermore, the real estate on a die surface is so precious that the circuitry is designed as close to the edges as possible. (The spacing is about tens of microns in the current practice.) Given that the stresses vary rapidly near the edges, a close examination of stress characteristics is required to explore design options that maximize the real estate on silicon while minimize the risk of damage.

The stress fields at bimaterial edges (Fig. 2) have been investigated for decades. The asymptotic analyses of Bogy [1] and others [2–5] showed that the stress field is singular near an edge. That is, when the distance from the edge r is small compared to other characteristic lengths of the geometry, the stress field scales as $Kr^{-\lambda}$. The exponent is in the range $0<\lambda<1$, depending on elastic moduli and wedge angles. The intensity factor K cannot be determined from the asymptotic analyses, but must be determined from a full field analysis for specific geometry and loading. A special case of two bonded quarter planes ($\theta_1 = \theta_2 = 90^\circ$ in Fig. 2) has been studied in detail for applications to joints of square plates [6, 7], and to adhesive layers between substrates [8–10]. The asymptotic field matches the full field in a zone about a tenth of the plate size or the adhesive thickness. If this zone is large enough to contain the volume where physical processes of interest occur, the asymptotic field provides useful information, and complements the numerical full-field analyses.

Figure 3(a) illustrates the geometry to be analyzed in this paper: a $2W_1 \times H_1$ silicon die on a $2W_2 \times H_2$ epoxy substrate. The substrate is typically fiber reinforced. The die is bonded to the substrate at a temperature ΔT above room temperature. Upon cooling, the thermal expansion misfit induces a stress field in the system. The left edge is enlarged in Fig. 3(b), where the two materials are denoted as 1 and 2. Both the die and the substrate are linearly thermoelastic, with E_j, ν_j and α_j (j = 1, 2) being Young's modulus, Poisson's ratio and the coefficient of thermal expansion. Unless otherwise stated, our analysis used the material constants listed in Table 1, and the dimensions $2W_1 = 20$ mm, $2W_2 = 22$ mm, $H_1 = 0.66$ mm, and $H_2 = 1.0$ mm. In this paper we remove the filler around the edges shown in Fig. 1. The significance of the filler will be studied elsewhere.

†To whom all correspondence should be addressed.

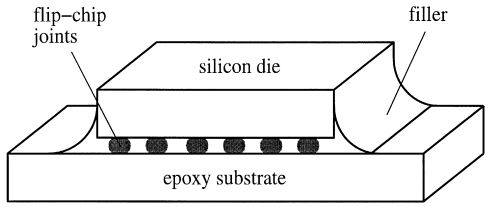

Fig. 1. Schematic of flip-chip packaging.

The feature size of an integrated circuit is on the order of 1 μm. Imperfections at edges have comparable sizes. No attempt is made here to include the individual features and imperfections in the analysis. The circuitry typically extends as close as 20–50 μm to a die edge. Consequently, we will focus on stress distribution over lengths between several times the feature size to hundreds of microns. This range roughly corresponds to $H_1/100<r<H_1/10$, where r is the distance from the die edge. Note that approximate analyses, such as those based on beam or shear-lag assumptions, are inadequate to resolve the stress field in this range.

Several studies have attempted to quantify near-edge stresses for this geometry, owing to its significance to electronic packaging. There are some confusions in the literature. It was claimed that even refined finite element meshes could not resolve the singular stress field [11]. The discrepancy made some researchers use a different intensity factor for each stress component [12, 13], or add a logarithmic singularity to the power singularity [12, 14]. None of such behaviors appear in the asymptotic analysis for the given material combinations.

For the geometry in Fig. 3(b), the asymptotic analysis of Hein and Erdogan [2] showed that often two singularity exponents exit, one giving a more singular stress field than the other. The physical significance of the split singularities is not well appreciated. It is often assumed that only the more singular field is significant. As will be shown in this paper, they hold the key to resolving the above controversies. The plan of this paper is as follows. Section 2 presents the stress fields obtained from finite element analyses. These results clearly show features that cannot be matched by the leading singularity. Section 3 recalls the split singularities from the asymptotic analysis, which shows that two

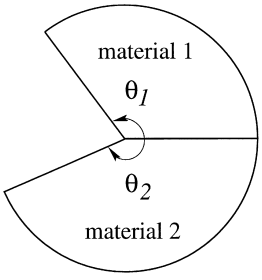

Fig. 2. Bonded wedges of dissimilar materials.

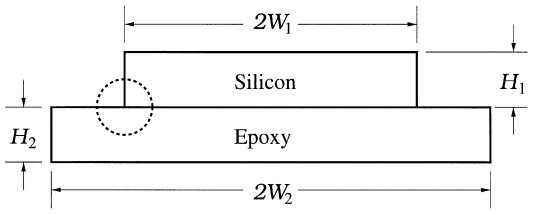

(a)

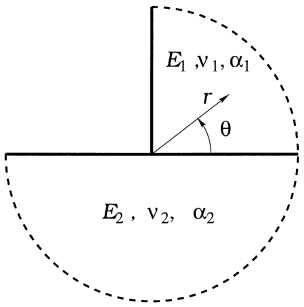

(b)

Fig. 3. Geometry used in calculations: (a) a silicon die on an epoxy substrate; (b) geometry near the die edge.

singularities correspond to two deformation modes. Once the two modes are superimposed, the asymptotic field matches the full field over a large zone. Section 4 presents the stress intensity factors for various material properties and specimen sizes.

2. FINITE ELEMENT SOLUTIONS

Finite element software ABAQUS was used to perform full field stress analysis. Due to the symmetry only the left half of the specimen need be analyzed. Figure 4 shows a typical mesh, consisting of 11 524 eight-node isoparametric elements and 35 547 nodes. Fine meshes were used near the edge to resolve the rapidly varying stress field. The feature size of an integrated circuit is on the order of 1 μm. Our continuum model cannot resolve stress below this length scale. Nonetheless in a few cases we used elements much less than 1 μm to ascertain that finite element analyses can resolve the asymptotic field. On the right boundary, which is the symmetry plane, roller boundary condition was applied to constrain the horizontal displacement. All other boundaries were traction-free. In the out-of-plane direction the generalized plane strain conditions were imposed. This paper does not treat the three-

Table 1. Material constants used for silicon and epoxy

Material	E (GPa)	ν	α ($\times 10^{-6}$/K)
Silicon	165	0.25	3.0
Epoxy	23.5	0.30	15.0

Table 2. λ_1 for various α and β combinations

λ_1	β								
	−0.4	−0.3	−0.2	−0.1	0.0	0.1	0.2	0.3	0.4
−0.9	0.200	0.287	0.342	0.381	0.411				
−0.8	0.205	0.293	0.348	0.387	0.416				
−0.7	0.208	0.299	0.355	0.393	0.421				
−0.6		0.305	0.360	0.398	0.426				
−0.5		0.310	0.366	0.404	0.431	0.452			
−0.4		0.314	0.371	0.409	0.436	0.456			
−0.3		0.316	0.376	0.414	0.441	0.461			
−0.2			0.381	0.420	0.446	0.465			
−0.1			0.385	0.424	0.451	0.469	0.483		
α 0.0			0.389	0.429	0.456	0.474	0.486		
0.1			0.392	0.434	0.460	0.478	0.489		
0.2				0.438	0.465	0.482	0.492		
0.3				0.443	0.469	0.486	0.495	0.499	
0.4				0.447	0.474	0.489	0.497	0.500	
0.5				0.450	0.478	0.493	0.499	0.499	
0.6					0.483	0.496	0.500	0.496	
0.7					0.487	0.499	0.499	0.488	0.463
0.8					0.491	0.500	0.492	0.456	
0.9					0.496	0.496			

dimensional field around the corner where two edges meet. The difference between the bonding temperature and room temperature was taken to be $\Delta T = 200$ K. The stresses are linearly proportional to the temperature drop.

On the interface plane there are two stress components: the shear and the peel stress. Figure 5(a) shows the finite element results of shear stress as a function of the distance from the edge. Epoxy has a higher thermal expansion coefficient than silicon. Were they unbonded, epoxy would contract more than silicon. The bonding constrains the relative motion, giving rise to the stress field. The whole system bends in the way shown in Fig. 4. Figure 5(a) also shows that the magnitude of the stress drops quickly with increasing distance from the edge, and increases with the epoxy stiffness. These qualitative trends may be expected from elementary considerations.

By contrast, the peel stress has some peculiar features [Fig. 5(b)]. It is compressive very close to the edge, becomes tensile at some location, attains a maximum, and then decreases. These features, which can be clearly seen in the case $E_2/E_1 = 0.142$, are pertinent to other curves in Fig. 5(b). Such a behavior cannot be interpreted by a single mode of singularity, since one singularity gives a monotonic variation of the stress with the distance from the edge. Also puzzling is that the peel stress very close to the edge is compressive.

Figure 6 plots stress distributions for various substrate thicknesses. As the substrate becomes thicker, the magnitude of the shear stress increases, but the magnitude of the peel stress decreases. Again, the trends very close to the edge cannot be interpreted by one mode of singularity.

Table 3. λ_2 for various α and β combinations

λ_2	β								
	−0.4	−0.3	−0.2	−0.1	0.0	0.1	0.2	0.3	0.4
−0.9	2.68×10^{-3}	1.33×10^{-3}	8.89×10^{-4}	6.67×10^{-4}	5.33×10^{-4}				
−0.8	1.14×10^{-2}	5.64×10^{-3}	3.75×10^{-3}	2.81×10^{-3}	2.25×10^{-3}				
−0.7	2.74×10^{-2}	1.34×10^{-2}	8.93×10^{-3}	6.70×10^{-3}	5.36×10^{-3}				
−0.6		2.52×10^{-2}	1.68×10^{-2}	1.26×10^{-2}	1.01×10^{-2}				
−0.5		4.15×10^{-2}	2.78×10^{-2}	2.09×10^{-2}	1.68×10^{-2}	1.40×10^{-2}			
−0.4		6.27×10^{-2}	4.22×10^{-2}	3.20×10^{-3}	2.57×10^{-2}	2.16×10^{-2}			
−0.3		8.90×10^{-2}	6.05×10^{-2}	4.61×10^{-2}	3.73×10^{-2}	3.14×10^{-2}			
−0.2			8.27×10^{-2}	6.37×10^{-2}	5.19×10^{-2}	4.39×10^{-2}			
−0.1			0.109	8.49×10^{-2}	6.99×10^{-2}	5.95×10^{-2}	5.18×10^{-2}		
α 0.0			0.139	0.110	9.15×10^{-2}	7.86×10^{-2}	6.90×10^{-2}		
0.1			0.173	0.138	0.117	0.102	9.01×10^{-2}		
0.2				0.170	0.146	0.129	0.116		
0.3				0.205	0.179	0.160	0.146	0.134	
0.4				0.244	0.215	0.195	0.181	0.170	
0.5				0.285	0.254	0.235	0.221	0.212	
0.6					0.297	0.278	0.267	0.262	
0.7					0.342	0.326	0.320	0.322	0.335
0.8					0.391	0.379	0.382	0.412	
0.9					0.443	0.441			

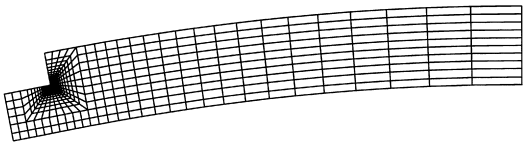

Fig. 4. A deformed finite element mesh, where displacements are magnified by a factor of 10.

3. SPLIT SINGULARITIES

To understand the nature of the near-edge stress field, we first recall a simpler situation: a homogeneous material with a wedge cut (Fig. 7). The problem was solved by Williams [15] and others [16–18]. The singular stress consists of a symmetric and an anti-symmetric mode, scaling with the distance r from the edge as, respectively, $r^{-\lambda_1}$ and $r^{-\lambda_2}$. Figure 7 plots the exponents λ_1 and λ_2 as functions of the wedge angle ψ. For a crack ($\psi = 0$), it is well known that both modes have the same exponent $\lambda = 1/2$. When $\psi > 0$, the one exponent splits into two, λ_1 and λ_2, *each* corresponding to *one* mode.

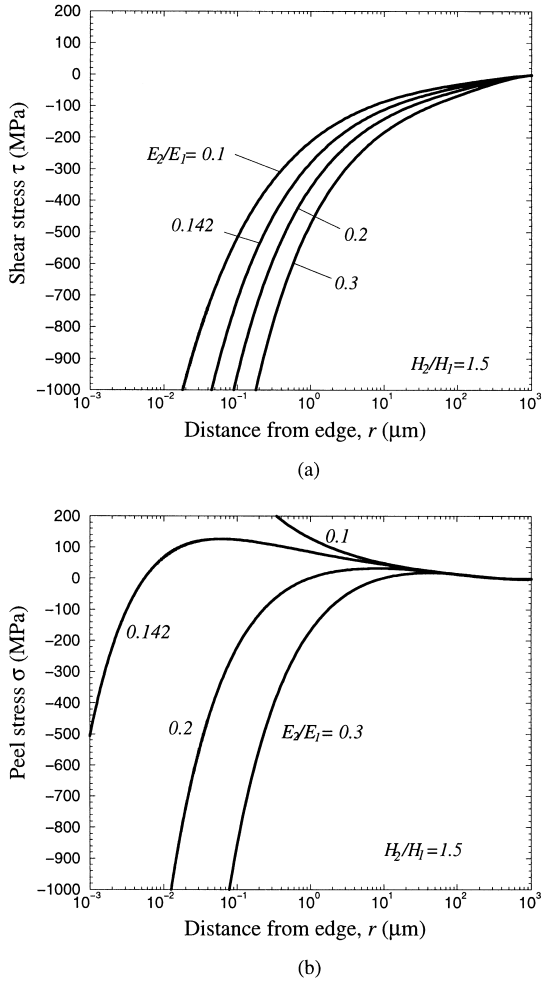

Fig. 5. Stress distributions on the interface for various substrate moduli: (a) shear stress; (b) peel stress.

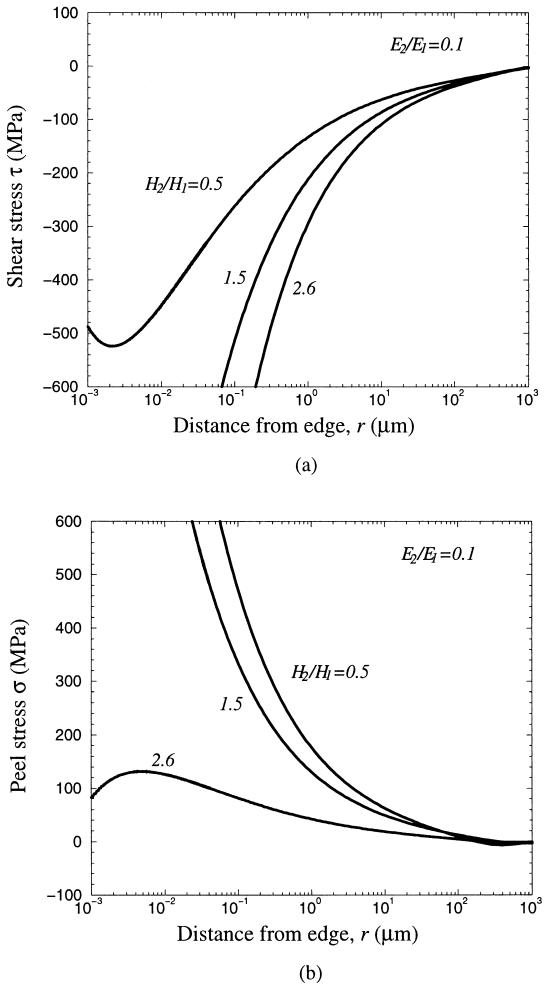

Fig. 6. Stress distributions on the interface for various substrate thicknesses: (a) shear stress; (b) peel stress.

The symmetric mode is more singular than the anti-symmetric mode. The weaker singularity (λ_2-singularity) cannot be neglected, for otherwise one cannot represent the shear stress on the bisection plane under general loading. Finite element calculations including both singularities have also been carried out [19, 20].

Now return to the configuration in Fig. 3(b), the edge of a die on a substrate. Appendix A gives details of the near-tip stress fields. Here we summarize the main features relevant to applications. The stress field has *two distinct* singularity exponents, each being associated with one mode. But now the modes cannot be classified into symmetric and anti-symmetric, because the configuration has no symmetry. The deformation is intrinsically of mixed mode, and the stress field is the superposition of the two modes. Let (r,θ) be the polar coordinates centered at the edge [Fig. 3(b)]. The components of the stress field are written in the form

$$\sigma_{ij}(r,\theta) = K_1 r^{-\lambda_1}\Sigma_{ij}^1(\theta) + K_2 r^{-\lambda_2}\Sigma_{ij}^2(\theta) \qquad (1)$$

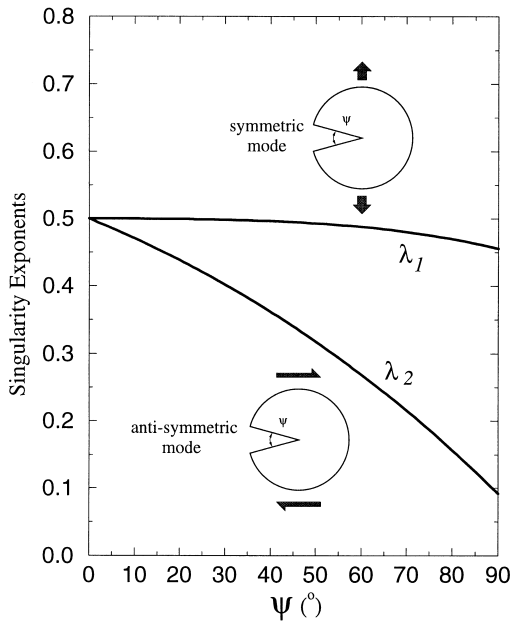

Fig. 7. Near a wedge cut in a homogeneous material, the singular field has two modes: the symmetric mode is more singular than the anti-symmetric mode.

where λ_1 and λ_2 are singularity exponents, K_1 and K_2 are the intensity factors, and $\Sigma_{ij}^1(\theta)$ and $\Sigma_{ij}^2(\theta)$ are angular distributions of the stresses. On the bimaterial interface the shear and peel stresses take the form

$$\tau = K_1 r^{-\lambda_1} + K_2 r^{-\lambda_2} \tag{2}$$

$$\sigma = \eta_1 K_1 r^{-\lambda_1} + \eta_2 K_2 r^{-\lambda_2}. \tag{3}$$

equation (2) defines K_1 and K_2. The dimensionless parameters η_1 and η_2 in equation (3) are discussed below.

Dundurs [23] introduced two parameters to characterize elastic mismatch of bimaterials:

$$\alpha = \frac{\mu_1(\kappa_2 + 1) - \mu_2(\kappa_1 + 1)}{\mu_1(\kappa_2 + 1) + \mu_2(\kappa_1 + 1)} \tag{4}$$

$$\beta = \frac{\mu_1(\kappa_2 - 1) - \mu_2(\kappa_1 - 1)}{\mu_1(\kappa_2 + 1) + \mu_2(\kappa_1 + 1)} \tag{5}$$

where κ_j is $(3 - \nu_j)/(1 + \nu_j)$ under plane stress conditions and $3 - 4\nu_j$ under plane strain conditions, and μ_j are the shear moduli, which relate to Young's modulus E_j as $\mu_j = E_j/[2(1 + \nu_j)]$. Here α should not be confused with the thermal expansion coefficient. Any pair of materials corresponds to a point on the α–β plane, within a parallelogram shown in Fig. 8. For our silicon–epoxy system, $\alpha = 0.744$ and $\beta = 0.206$.

Bogy [1] presented the leading singularity exponent on the α–β plane. Hein and Erdogan [2] found all the singularity exponents, but presented them as a function of Young's modulus ratio for fixed Poisson ratios. For completeness both singularity exponents are presented on the α–β plane in Fig. 8. Data collected by Suga [24] on over 100 material pairs suggest that for the majority of material combinations α is confined to the range $-0.7 < \alpha < 0.7$. In this range there are always two distinct modes of singularities. For the case of a stiff material on a soft one ($\alpha > 0$ and $\beta > 0$), the leading singularity λ_1 is in the range between 0.456 and 0.5, and the second singularity exponent is in the range $0.07 < \lambda_2 < \lambda_1$. The maximum singularity exponent (0.5) occurs on the line $2\beta = 1 - \alpha$. For our silicon–epoxy system, $\lambda_1 = 0.497$ and $\lambda_2 = 0.346$.

When (α,β) falls into the up-right triangle region in Fig. 8 where no contour of constant singularity exponent enters, the singularity exponents are a pair of complex conjugate numbers. On one side of the triangle, across which the two real exponents become a complex conjugate pair, the two real exponents degenerate to one real exponent. The degeneracy leads to an additional logrithmic singularity [1]. In this paper we do not study these

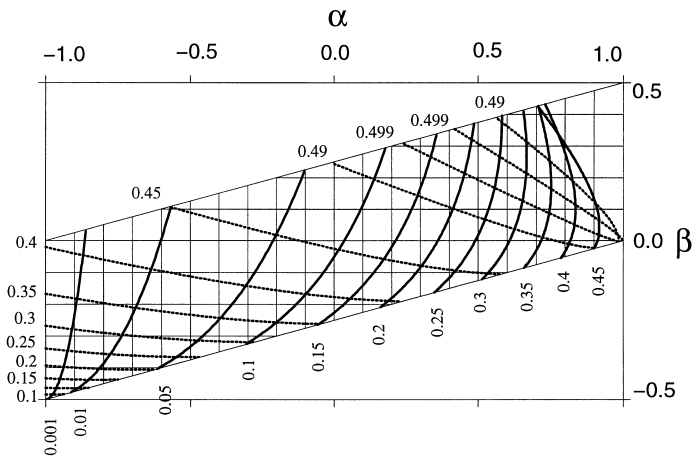

Fig. 8. Contours of constant singularity exponents on the plane of the Dundurs parameters α and β. The contour values for solid lines are labeled vertically; those for dotted lines horizontally.

Table 4. η_1 for various α and β combinations

η_1	β								
	−0.4	−0.3	−0.2	−0.1	0.0	0.1	0.2	0.3	0.4
−0.9	5.65	3.47	2.68	2.25	1.97				
−0.8	5.93	3.51	2.68	2.24	1.95				
−0.7	6.40	3.56	2.68	2.23	1.94				
−0.6		3.64	2.70	2.22	1.92				
−0.5		3.75	2.72	2.22	1.91	1.69			
−0.4		3.91	2.75	2.21	1.89	1.67			
−0.3		1.83	2.79	2.22	1.88	1.65			
−0.2			1.98	2.22	1.87	1.63			
−0.1			2.93	1.94	1.85	1.60	1.42		
α 0.0			3.05	2.25	1.84	1.58	1.38		
0.1			3.23	2.28	1.83	1.72	1.34		
0.2				2.32	1.82	1.51	1.57		
0.3				2.38	1.81	1.48	1.25	1.40	
0.4				2.48	1.79	1.43	1.19	1.00	
0.5				2.65	1.78	1.37	1.11	0.905	
0.6					1.77	1.30	1.00	0.777	
0.7					1.76	1.18	0.846	0.584	0.331
0.8					1.75	1.00	0.582	0.141	
0.9					1.74	0.580			

behaviors because the (α,β) range is outside the material combination of interest to us.

The asymptotic analysis also determines the coefficients η_1 and η_2, which depend on the Dundurs parameters; see Tables 4 and 5 for their values. For the silicon–epoxy system $\eta_1 = 0.731$ and $\eta_2 = -0.906$. Note that $\eta_1 > 0$ and $\eta_2 < 0$ for all the material combinations studied. Now the peculiar features of the peel stress found in the finite element analyses [see Fig. 5(b)] can be readily interpreted in terms of the asymptotic analysis. For the stress very close to the edge, the leading singularity dominates. Since the shear stress is negative, $K_1 < 0$ according to equation (2). Together with $\eta_1 > 0$, equation (3) dictates that the peel stress at the tip should be compressive. As r increases, the second singularity becomes important; a negative η_2 suggests the peel stress can change sign and becomes tensile.

4. STRESS INTENSITY FACTORS

We use the modulus and thickness of silicon die to normalize all results, and examine the effect of varying substrate modulus and thickness. The stress intensity factors defined above have dimensions $K_1 \sim [\text{stress}] \times [\text{length}]^{\lambda_1}$ and $K_2 \sim [\text{stress} \times [\text{length}]^{\lambda_2}$, and are linear in the temperature change ΔT. Consequently, they take the form

$$K_1 = k_1 E_1' \Delta\alpha \Delta T H_1^{\lambda_1} \tag{6}$$

$$K_2 = k_2 E_1' \Delta\alpha \Delta T H_1^{\lambda_2} \tag{7}$$

where $E_1' = E_1/(1-\nu_1)$ and $\Delta\alpha$ is the difference in the thermal expansion coefficients between epoxy and silicon. The dimensionless numbers k_1 and k_2 depend on various dimensionless ratios. For thin dies and substrates and Poisson's ratios given in

Table 5. η_2 for various α and β combinations

η_2	β								
	−0.4	−0.3	−0.2	−0.1	0.0	0.1	0.2	0.3	0.4
−0.9	−68.4	−63.7	−62.3	−61.6	−61.2				
−0.8	−38.4	−32.5	−30.9	−30.2	−29.8				
−0.7	−30.5	−22.2	−20.5	−19.7	−19.3				
−0.6		−17.3	−15.3	−14.5	−14.0				
−0.5		−14.6	−12.2	−11.3	−10.9	−10.6			
−0.4		−13.1	−10.2	−9.26	−8.76	−8.45			
−0.3		−5.74	−8.89	−7.79	−7.25	−6.93			
−0.2			−6.06	−6.70	−6.12	−5.79			
−0.1			−7.32	−5.43	−5.25	−4.89	−4.66		
α 0.0			−6.95	−5.26	−4.57	−4.18	−3.94		
0.1			−6.85	−4.78	−4.02	−3.70	−3.34		
0.2				−4.42	−3.56	−3.12	−2.91		
0.3				−4.17	−3.19	−2.71	−2.42	−2.21	
0.4				−4.02	−2.88	−2.36	−2.05	−1.83	
0.5				−4.02	−2.62	−2.05	−1.72	−1.48	
0.6					−2.40	−1.76	−1.40	−1.15	
0.7					−2.20	−1.48	−1.08	−0.797	−0.530
0.8					−2.03	−1.15	−0.693	−0.235	
0.9					−1.87	−0.622			

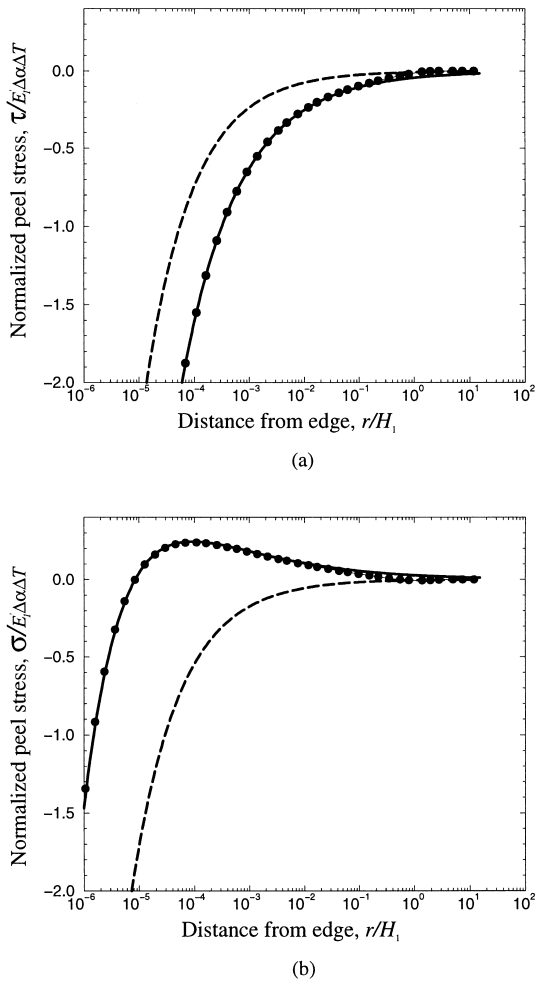

Fig. 9. Comparison of results from the finite element calculation and the singular stress analysis. Solid line is singular stress solution of combined two modes. Finite element results are shown in filled circles. The dashed line is the contribution of the λ_1-singularity alone: (a) shear stress; (b) peel stress.

Table 1, k_1 and k_2 only depend on the thickness ratio H_2/H_1 and Young's modulus ratio E_2/E_1.

The stress intensity factors for specific geometry and loading were determined as follows. A finite element analysis gave a full field solution. The calculated stresses close to the edge, say $10^{-4}<r/H_1<10^{-2}$, were used to fit equations (2) and (3), with the stress intensity factors as the fitting parameters. A least-square fitting procedure was used. A more sophisticated finite element method has been described to compute the stress intensity factors [21, 22].

Figure 9 compares the finite element results and the asymptotic distributions (2) and (3). The normalized stress intensity factors, $k_1 = -7.7 \times 10^{-3}$ and $k_2 = -3.6 \times 10^{-2}$, best fit the asymptotic solutions to the finite element results. The asymptotic field matches with the full field in the region about ten percent of the die thickness H_1. In matching the asymptotic and the full field, we only used the two numbers—the intensity factors—as the adjustable parameters. We only used finite element results in the range $10^{-4}<r/H_1<10^{-2}$. The resulting fit extends to a much larger range, at least between $10^{-8}<r/H_1<10^{-1}$, the lower bound being limited by our finite element mesh size. When r/H_1 is sufficiently large, the singular field gives way to a non-singular field. Appendix A shows that, for our problem, the leading non-singular term in the asymptotic expansion vanishes.

In Fig. 9 the dashed line is the contribution of the $r^{-\lambda_1}$ singularity alone. It does not fit the finite element results in the entire zone of physical relevance. This behavior is understood as follows. We use the peel stress (3) in this dicussion; the conclusion for the shear stress is qualitatively the same. The ratio of the λ_1-singular stress to the λ_2-singular stress is

$$R = \frac{|\eta_1 K_1| r^{-\lambda_1}}{|\eta_2 K_2| r^{-\lambda_2}} = \left|\frac{\eta_1 k_1}{\eta_2 k_2}\right| \left(\frac{H_1}{r}\right)^{\lambda_1 - \lambda_2}. \qquad (8)$$

When r is small, λ_1-singularity dominates. For parameters specified in Table 1, $|\eta_1 k_1/\eta_2 k_2| = 0.16$ and $\lambda_1 - \lambda_2 = 0.15$, both of which are so small that λ_1-singularity dominates in an exceedingly small zone, $r/H_1<10^{-6}$. (With $H_1 = 1$ mm, $r/H_1 = 10^{-6}$ corresponds to $r = 1$ nm.) Such a small range is of no practical interest. Figure 10 draws a map of $\log(r/H_1)$ vs $\log R$. For a given geometry, each bimaterial gives a straight line on the map. Specify a reference value R_c. If $R > R_c$, λ_1-singularity dominates. If $R<1/R_c$, λ_2-singularity dominates. In the range of r/H_1 such that $1/R_c<R<R_c$, the two singularities are of comparable importance. For example, take $R_c = 2$ in Fig. 10 and look at the material combination of $E_2/E_1 = 0.2$. The λ_1-singularity dominates in the range $r/H_1<4 \times 10^{-5}$, and the λ_2-singularity dominates in the range $r/H_1 > 3 \times 10^{-1}$. Either one is outside the range of practical significance. In the range of $4 \times 10^{-5}<r/H_1<3 \times 10^{-1}$ the two modes have comparable contributions.

Figures 5 and 6 have shown that interfacial stress distributions vary substantially with the thickness and modulus of the polymer substrate. We carried out more extensive finite element analyses for a range of substrate thickness and modulus. Limited space here does not allow us to plot all the stress distributions. The reader, however, can plot them for the substrate of interest by the following procedure. Figure 11 gives the stress intensity factors for various substrate thickness and modulus, which were obtained by fitting the asymptotic and the full field as discussed above. Use equations (2) and (3) to plot the shear and peel stress distributions, the locations of the relevant parameters being listed in Table 6. The temperature change and thermal expansion coefficients enter through equations (6) and (7). In this paper we have emphasized the stress

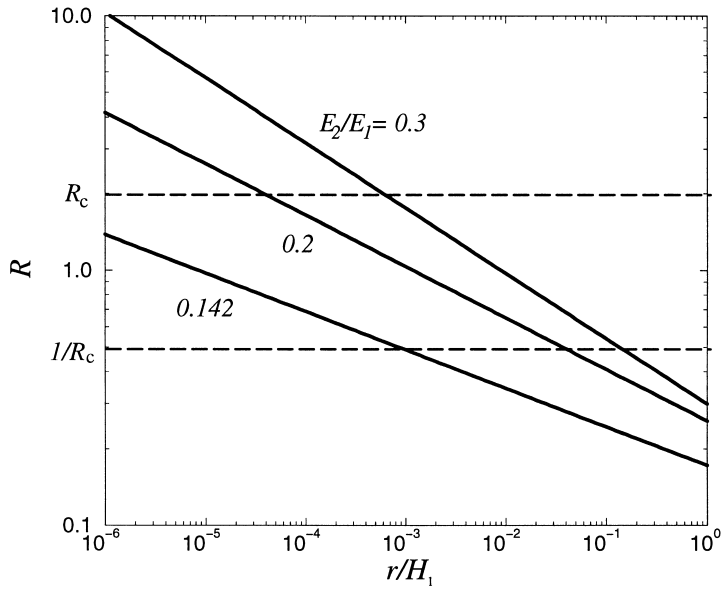

Fig. 10. The map of singular mode domination for the geometry in Fig. 3(a) with $H_2/H_1 = 1.5$.

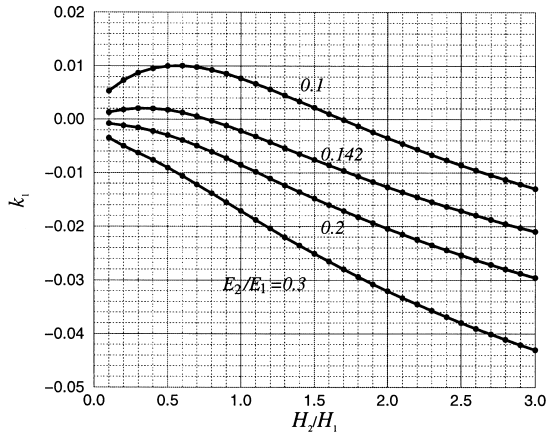

(a)

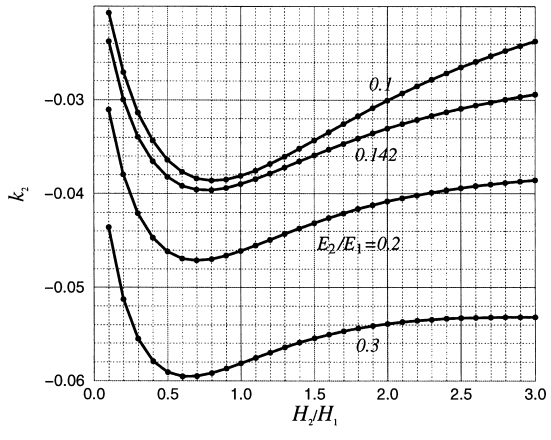

(b)

Fig. 11. The normalized stress intensity factors as functions of thickness ratio H_2/H_1 and modulus ratio E_2/E_1: (a) k_1; (b) k_2.

components on the interface. Should the stress components inside the die or substrate be of interest, one can plot equation (1) using the angular functions Σ_{ij}^1 and Σ_{ij}^2 described in Appendix A.

5. CONCLUSIONS

A silicon die on a polymer packaging substrate is susceptible to debonding at edges, where thermal stress concentrates. The problem is of particular concern because, to maximize the real estate on silicon, current designs place the circuitry very close to the edges. This paper focuses on the shear and the peel stress on the interface, at a distance a small fraction of the die thickness from an edge. A finite element analysis gives full stress field. An asymptotic analysis shows that the near-edge stress field consists of two modes, one being more singular than the other. The full field is then compared with the asymptotic field. When the more singular mode is used alone, the asymptotic field matches the full field in an exceedingly small zone, which is of no practical interest. When both singular modes are superimposed, the asymptotic field matches the full

Table 6. Dependence of the nondimensional constants in the singular stresses (2) and (3) and the stress intensity factors (6) and (7) on elastic constants (the Dundurs parameters α, β) and thickness ratio (H_2/H_1)

	λ_1	λ_2	η_1	η_2	k_1	k_2
α, β	Table 2	Table 3	Table 4	Table 5	Fig. 11	Fig. 11
H_2/H_1	†	†	†	†	Fig. 11	Fig. 11

†No dependence.

field within a zone about a tenth of the die thickness. The finding clearly demonstrates the practical significance of the split singularities, which have hitherto caused confusions in the literature on electronic packaging. The paper describes a procedure to plot the near edge stress field for large ranges of substrate modulus, thickness and thermal expansion coefficient. The stress field obtained here for an idealized geometry can be used as a reference in studying the effects of fillers and die edge shapes, and as the background load in studying the failure mechanisms and material nonlinearity at the scale of individual features.

Acknowledgements—The work was supported by the Institute of Materials Research and Engineering, Singapore, by Intel Corporation, and by DARPA (N6001-98-1-8916).

REFERENCES

1. Bogy, D. B., *J. appl. Mech.*, 1971, **38**, 377.
2. Hein, V. L. and Erdogan, F., *Int. J. Fract.*, 1971, **7**, 317.
3. Rao, A. K., *Z. angew. Math. Mech.*, 1971, **51**, 395.
4. Gdoutos, E. E. and Theocaris, P. S., *J. appl. Mech.*, 1975, **42**, 688.
5. Dempsey, J. P. and Sinclair, G. B., *J. Elasticity*, 1981, **11**, 317.
6. Mizuno, K., Miyazawa, K. and Suga, T., *J. Faculty Engng*, 1988, **39**, 401.
7. Munz, D. and Yang, Y. Y., *J. appl. Mech.*, 1992, **59**, 857.
8. Reedy, E. D. Jr, *Engng Fract. Mech.*, 1990, **36**, 575.
9. Reedy, E. D. Jr, *Int. J. Solids Struct.*, 1993, **30**, 767.
10. Jiang, Z. Q., Huang, Y. and Chandra, A., *J. Electron. Packaging*, 1997, **119**, 127.
11. Madenci, E. and Shkarayev, S., *Application of Fracture Mechanics in Electronic Packaging*, AMD-Vol. 222/EEP-Vol. 20, 1997, p. 61.
12. Yuuki, R., Xu, J.-Q. and Kayama, N., *Advances in Electronic Packaging*, EEP-Vol. 4-1, 1993, p. 119.
13. Hu, J. M., *Application of Fracture Mechanics in Electronic Packaging and Materials*, EEP-Vol. 11/MD-Vol. 64, 1995, p. 13.
14. Yu, Q. and Shiratori, M., *Advances in Electronic Packaging*, EEP-Vol. 10-1, 1995, p. 389.
15. Williams, M. L., *J. appl. Mech.*, 1952, **74**, 526.
16. Carpenter, W. C., *Int. J. Fract.*, 1984, **26**, 201.
17. Sinclair, G. B., Okajima, M. and Griffin, J. H., *Int. J. Num. Meth. Engng*, 1984, **20**, 999.
18. Hills, D. A., as quoted by Barber, J. R., in *Elasticity*. Kluwer Academic, Dordrecht, 1992, p. 132.
19. Andersson, B., Falk, U., Babuska, I. and von Petersdorff, T., *Int. J. Num. Meth. Engng*, 1995, **38**, 2135.
20. Yosibash, Z., *Int. J. Num. Meth. Engng*, 1997, **40**, 4611.
21. Babuska, I., von Petersdorff, T. and Andersson, B., *SIAM J. Numer. Anal.*, 1994, **31**, 1265.
22. Andersson, B., Babuska, I. and Falk, U., *Proc. 17th Congress of the International Council of the Aeronautical Sciences*, Paper No. ICAS-90-4.9.2, 1990, p. 1730.
23. Dundurs, J., in *Mathematical Theory of Dislocations*. American Society of Mechanical Engineering, New York, 1969, p. 70.
24. Suga, T., Ph.D. thesis, University of Stuttgart, 1984.
25. Timoshenko, S. and Goodier, J. N., *Theory of Elasticity*. McGraw-Hill, New York, 1951.
26. Munz, D., Fett, T. and Yang, Y. Y., *Engng Fract. Mech.*, 1993, **44**, 185.

APPENDIX A

Interface corner stress field

For a wide range of wedge angles and bimaterial combinations, the stress field around a corner can be written as

$$\sigma_{ij}(r,\theta) = K_1 r^{-\lambda_1}\Sigma_{ij}^1(\theta) + K_2 r^{-\lambda_2}\Sigma_{ij}^2(\theta) + \sigma_{ij}^0 + o(1). \quad \text{(A1)}$$

Here σ_{ij}^0 is the constant stress term, and the term $o(1)$ approaches zero as the edge is approached.

A.1. Singular stress

The method of Airy functions can be found in a standard textbook [25]. Let (r,θ) be the polar coordinates centered at the edge. The Airy functions are chosen of a separable form

$$\phi_j = r^{-\lambda+2}F_j(\theta) \quad \text{(A2)}$$

where $j = 1,2$ represents the quarter and the half planes, respectively. The biharmonic equation $\nabla^4\phi_j = 0$ dictates that for $\lambda \neq 0,2$ the angular function should take the form

$$F_j(\theta) = a_j \sin(\lambda-2)\theta + b_j \cos(\lambda-2)\theta + c_j \sin\lambda\theta + d_j \cos\lambda\theta. \quad \text{(A3)}$$

The constants a_j, b_j, c_j and d_j are to be determined by boundary conditions. The stresses relate to the Airy functions as

$$\sigma_r = \frac{1}{r^2}\frac{\partial^2\phi_j}{\partial\theta^2} + \frac{1}{r}\frac{\partial\phi_j}{\partial r} = r^{-\lambda}[F_j''(\theta) - (\lambda-2)F_j(\theta)],$$

$$\sigma_\theta = \frac{\partial^2\phi_j}{\partial r^2} = r^{-\lambda}(\lambda-1)(\lambda-2)F_j(\theta),$$

$$\tau_{r\theta} = -\frac{\partial}{\partial r}\left(\frac{1}{r}\frac{\partial\phi_j}{\partial\theta}\right) = r^{-\lambda}(\lambda-1)F_j'(\theta). \quad \text{(A4)}$$

The displacements are given by

$$2\mu_j u_r = r^{-\lambda+1}[(\lambda-2)F_j(\theta) + (\kappa_j+1)(c_j\sin\lambda\theta + d_j\cos\lambda\theta)],$$

$$2\mu_j u_\theta = r^{-\lambda+1}[-F_j'(\theta) + (\kappa_j+1)(c_j\cos\lambda\theta - d_j\sin\lambda\theta)] \quad \text{(A5)}$$

where μ_j are shear moduli, κ_j is $(3-\nu_j)/(1+\nu_j)$ for plane stress and $3-4\nu_j$ for plane strain. The boundary conditions are:

1. traction free at the surface of material 1: $\sigma_\theta = \tau_{r\theta} = 0$, for $\theta = \pi/2$;
2. traction free at the surface of material 2: $\sigma_\theta = \tau_{r\theta} = 0$, for $\theta = -\pi$;
3. stresses σ_θ, $\tau_{r\theta}$ and displacements u_r, u_θ are continuous at the interface ($\theta = 0$).

The boundary conditions give the following eigenvalue problem:

$$
\begin{aligned}
&-a_1 \sin \lambda\pi/2 - b_1 \cos \lambda\pi/2 + c_1 \sin \lambda\pi/2 + d_1 \cos \lambda\pi/2 = 0,\\
&-a_1(\lambda-2)\cos \lambda\pi/2 + b_1(\lambda-2)\sin \lambda\pi/2\\
&+c_1\lambda \cos \lambda\pi/2 - d_1\lambda \sin \lambda\pi/2 = 0,\\
&-a_2 \sin \lambda\pi + b_2 \cos \lambda\pi - c_2 \sin \lambda\pi + d_2 \cos \lambda\pi = 0,\\
&a_2(\lambda-2)\cos \lambda\pi + b_2(\lambda-2)\sin \lambda\pi + c_2\lambda \cos \lambda\pi\\
&+d_2\lambda \sin \lambda\pi = 0,\ b_1 + d_1 = b_2 + d_2,\\
&a_1(\lambda-2) + c_1\lambda = a_2(\lambda-2) + c_2\lambda,\\
&\mu_2[b_1(\lambda-2) + d_1(\lambda+\kappa_1-1)]\\
&= \mu_1[b_2(\lambda-2) + d_2(\lambda+\kappa_2-1)],\\
&\mu_2[a_1(\lambda-2) + c_1(\lambda-\kappa_1-1)]\\
&= \mu_1[a_2(\lambda-2) + c_2(\lambda-\kappa_2-1)]. \qquad \text{(A6)}
\end{aligned}
$$

For a nontrivial solution of the constants a_j, b_j, c_j and d_j, the determinant of equation (A6) must vanish. After algebraic simplification, one has a transcendental equation for λ [1, 5]:

$$
\begin{aligned}
&4(1+\beta)\sin^2(\lambda\pi)[(1-\beta)\cos^2(\lambda\pi/2) + (\beta-\alpha)(1-\lambda)^2]\\
&\quad - 2(1-\alpha)\sin^2(\lambda\pi) - (1+\alpha)^2[\cos^2(\lambda\pi/2)\\
&\quad - (1-\lambda)^2] = 0 \qquad \text{(A7)}
\end{aligned}
$$

where α and β are the Dundurs parameters. The singularity exponents λ_1 and λ_2, which are restricted between 0 and 1, are the two roots of the equation.

For each eigenvalue, λ_1 or λ_2, equation (A6) can be solved for the eigenvector $(a_1, \ldots, d_2)$. This yields the singular field up to two constants, which are denoted as K_1 and K_2. The angular functions are normalized such that $\Sigma^1_{r\theta}(0) = \Sigma^2_{r\theta}(0) = 1$. On the interface, the ratio of the peel to the shear stress gives

$$\eta = \frac{(b_1 + d_1)(\lambda-2)}{a_1(\lambda-2) + c_1\lambda}. \qquad \text{(A8)}$$

This yields the coefficients η_1 and η_2 from λ_1 and λ_2. The asymptotic analysis does not determine K_1 and K_2.

A.2. Constant stress term

To get the constant stress term under thermal loading, we choose $\lambda = 0$ in the Airy function (A2). The F_j in the Airy function becomes

$$F_j(\theta) = a_j \sin 2\theta + b_j \cos 2\theta + c_j\theta + d_j \qquad \text{(A9)}$$

and the stresses are

$$
\begin{aligned}
\sigma_r &= -2a_j \sin 2\theta - 2b_j \cos 2\theta + 2d_j,\\
\sigma_\theta &= 2a_j \sin 2\theta + 2b_j \cos 2\theta + 2d_j,\\
\tau_{r\theta} &= -2a_j \cos 2\theta + 2b_j \sin 2\theta. \qquad \text{(A10)}
\end{aligned}
$$

The thermoelastic relation is

$$
\begin{aligned}
2\mu_j(\varepsilon_r - \bar{\alpha}_j\Delta T) &= \sigma_r - (3-\kappa_j)(\sigma_r + \sigma_\theta)/4,\\
2\mu_j(\varepsilon_\theta - \bar{\alpha}_j\Delta T) &= \sigma_\theta - (3-\kappa_j)(\sigma_\theta + \sigma_r)/4,\\
2\mu_j\varepsilon_{r\theta} &= \tau_{r\theta}
\end{aligned}
$$

where $\bar{\alpha}_j$ is α_j for plane stress and is $(1+\nu_j)\alpha_j$ for plane strain. (The coefficients of thermal expansion α_j should not be confused with the Dundurs parameter α.) The strains are expressed in displacements in the usual way

$$\varepsilon_r = \frac{\partial u}{\partial r},\ \varepsilon_\theta = \frac{u}{r} + \frac{1}{r}\frac{\partial v}{\partial \theta},\ \varepsilon_{r\theta} = \frac{1}{r}\frac{\partial u}{\partial \theta} + \frac{\partial v}{\partial r} - \frac{v}{r}. \qquad \text{(A12)}$$

After inserting the stresses and the strains into the thermoelastic relation, the displacements are found by integration

$$
\begin{aligned}
u/r &= \bar{\alpha}\Delta T + [-2a_j \sin 2\theta - 2b_j \cos 2\theta + (\kappa_j - 1)d_j]/2\mu_j\\
&\quad + U_j \cos\theta + V_j \sin\theta,\\
v/r &= (-2a_j \cos 2\theta + 2b_j \sin 2\theta)/2\mu_j - U_j \sin\theta\\
&\quad + V_j \cos\theta + \Omega_j. \qquad \text{(A13)}
\end{aligned}
$$

The constants U_j and V_j represent the in-plane translations and Ω_j is the rotation about the edge. They can be taken to be zero without affecting the stresses. The same boundary conditions as in Section A.1 are applied to obtain a_j, b_j and d_j. They are all found to be zero. Therefore, the constant stress term $\sigma^0_{ij} = 0$ for our wedge geometry. By contrast, at the corner of two jointed quarter planes, the constant stress term is non-zero [6, 7, 26].